POLYSTAR: A PROCEDURE FOR SPECTRAL DECOMPOSITION OF IUE LINE-BY-LINE (SPATIALLY RESOLVED) DATA

Bruce Altner
Applied Research Corporation
Landover, MD 20785

1 Introduction

The majority of the targets observed by IUE are point sources, *i.e.*, individual stars, quasi-stellar objects, etc. For such objects the analyst usually does not need to examine the line-by line (LBL) data file, which is always included on the GO tape along with the MELO spectrum (see next section for a description of LBL data). However, in order to separate the overlapping profiles of individual stars in globular cluster center-of-light images Altner (1988a) developed the POLYSTAR procedure. This report describes some of the specific features of POLYSTAR, as well as some general characteristics of IUE spatially resolved data. Most of the examples discussed here pertain to the SWP camera, but the procedure works equally well with either of the three IUE cameras. Recent applications of POLYSTAR beyond its originally intended use with the globular cluster spectra include the analysis of individual knots in the starburst galaxy NGC 1068 (Bruhweiler and Altner 1988), identification of the star Sk -69 202 as the progenitor of the LMC supernova SN 1987A (Sonneborn, Altner and Kirshner 1987), ultraviolet spectroscopy of point-like and extended features in the LINERs NGC 3998 and NGC 404 (Reichert *et al.* 1988) and a study of the gravitationally lensed double quasar 0957 +561 (Altner and Heap 1988). Because of its proven usefulness in a these and other areas of IUE research, POLYSTAR is presently being added to the Goddard RDAF library of standard analysis routines and will soon be available for use by visiting GOs.

2 Spatial Resolution with IUE

The IUE "spatial axis" is nearly parallel to the long axis of the large aperture ($21''.4 \times 10''$) and almost perpendicular to the dispersion direction (hence, it is also called the cross-dispersion axis). Since the instrumental response to a point source in the short wavelength spectrograph ranges between $4''.6$ and $6''.0$ (FWHM) under conditions of optimum focus (Cassatella, Barbero, and Benvenuti 1985; hereafter CBB), one can expect to resolve discrete sources if they are not too close together.[1]

2.1 LBL versus ELBL

As of October 1, 1985 the IUESIPS software which generates the LBL files and records them on the GO tapes was changed. An "extended" line-by-line (ELBL) format replaced the earlier LBL structure. This was done to improve the spatial resolution of IUE low

[1] "Too close" means a separation less than 0.849 times the FWHM between stars in the aperture, according to CBB. This value derives from the Rayleigh criterion, which specifies the minimum separation at which an analytical minimum might be found between two peaks of equal intensity. However, in §3.2.2 we will show that by making certain assumptions about the system it is sometimes possible to spatially resolve peaks separated by distances smaller than the Rayleigh limit.

QUANTITY	LBL	ELBL
1 pixel	$\sqrt{2}/2$	$\sqrt{2}$
1 dpx	1.00	2.00
$1''$	0.47	0.94
σ_{1350}	0.92	1.83
σ_{1850}	1.18	2.37
FWHM_{1350}	2.16	4.31
FWHM_{1850}	2.79	5.58

Table 1: Values of several frequently discussed variables and dimensions, in units of "lines". Note that an ELBL line is half the size of an LBL line, so there are always twice as many of them in any measure. The FWHM and σ values quoted refer to conditions of optimum focus.

dispersion data; instead of 55 lines in the LBL file, the investigator now has 110 ELBL lines, effectively doubling the resolution of the data. This was possible because of the removal of a step in the processing software which averaged adjacent points in the earlier version. Thus, the ELBL data had always been available but had been degraded to the LBL format in the interests of improving the signal-to-noise of the data. A full discussion of the philosophy behind this change, and its implementation, is given by Muñoz Peiro (1985). For our purposes here the doubling of the number of lines in the spatially resolved files is the most important change associated with the new software. Henceforward, we shall use the term "LBL" to represent both line-by-line and extended line-by-line spatially resolved files, unless it becomes important to distinguish the two in a given context. IUESIPS usually centers the line of peak signal intensity within the available range of lines, so profiles centered near line 27 are from LBL data, while profiles centered near line 55 are assuredly from ELBL files.

The most convenient unit of measure for discussing the spatial resolution properties of IUE data is the "line", as we have used the term in the above discussion. In reality, these lines are the boundaries of diagonal pixels (1 dpx = $\sqrt{2}$ pixels) in the LBL files (Turnrose and Harvel 1980), or half diagonals ($\sqrt{2}/2$ pixels) in the ELBL format. The transformation between other units (*i.e.*, arcseconds, pixels and diagonal pixels) and line units can sometimes be confusing (even to those with some experience handling them), so we present in Table 1 values of some of the quantities which are important in discussions of the spatially resolved data. The conversion to arcseconds is based on the $1''.51$/pixel plate scale derived by Panek (1982) for the SWP camera.

2.2 Cross-dispersion Profiles

The distribution of sources along the IUE spatial axis is, in fact, really a projection of their true positions in the large aperture.[2] We illustrate this in Fig. 1*a–c* for an hypothetical grouping of three stars. For the purposes of this illustration we have arbitrarily placed the three stars as shown in Fig. 1*a*, where north is up and east is to the left, *e.g.*, as they would appear on the plane of the sky. The stars are assumed to have a brightness ratio of 3:2:1 in the wavelength interval 1400–1600 Å. What would the cross-dispersion profile in this wavelength range look like for these stars? The answer, of course, depends upon the relative orientation of the large aperture, which is a function of the sun's position as well as the target coordinates. During the course of a year the aperture will rotate through a full 360° for any celestial object not too close to the ecliptic. Here we adopt the convention

[2]See Altner 1988b for a discussion of how two observations of the same multi-component field can be used to derived two-dimensional information about the source positions, rather than just projected separations.

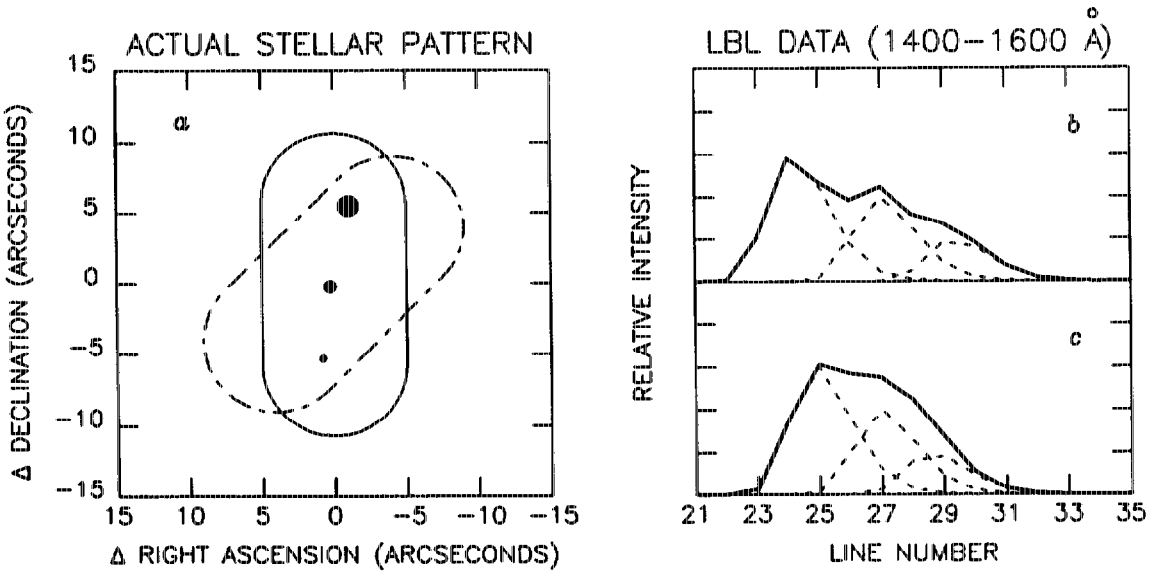

Figure 1: Hypothetical distribution of three stars and the resulting LBL profiles they would produce at two different orientations of the IUE large aperture. *a*) PA=0 and 315 for the apertures drawn with solid line and dash-dotted line, respectively. North is up, east is to the left; *b*) modeled spatial profile at PA=0 (heavy line), which is the sum of the three individual star profiles (dotted lines); *c*) same as *b*), but for PA=315.

used by Sonneborn *et al.* (1987) for describing the position angle of the large aperture, that is

$$\text{PA} = 73^\circ - \text{spacecraft roll angle} \qquad (1)$$

where PA is 0 for a due north pointing and 90 for a due east pointing.[3] The spacecraft roll angle is recorded on the observer scripts at the time of observation or can be calculated for a specific date using the equation given in Sonneborn *et al.* (1987). We note in Fig. 1*a* that two aperture orientations are depicted. The aperture drawn with a solid line is at PA=0 while that drawn with a dash-dotted line is at PA=315.

The resulting cross-dispersion profiles, modeled using the PSF parameters given by CBB in this wavelength range (and assuming perfect focus), are depicted using a heavy solid line in Fig. 1*b* (PA=0) and Fig. 1*c* (PA=315). Individual profiles (dotted lines) reflect the assumed 3:2:1 brightness ratio. Note that the relative separations between the individual peaks are different in the two cases. These are *projected* separations, measured along the cross-dispersion axis, which is rotated with respect to the aperture's "major axis" by 9° (see Turnrose and Thompson 1984, their Section 7.2.2). Although included here for illustration only, the modeled profiles are quite realistic representations of typical multi-source profiles (see also Fig. 3).

[3]The two ends of the symmetrical aperture can be distinguished from each other by noting that one is further from the small aperture plate than the other (see Fig. 6a in Sonneborn *et al.* 1987). By convention, this is the north-pointing end at PA=0.

3 POLYSTAR

The POLYSTAR program performs a simultaneous non-linear least-squares fit to the spatially resolved data, assuming there are N sources in the large aperture. The fitting routine at the heart of the procedure is adapted from the CURFIT algorithm in Chapter 11 of Bevington (1969), with the addition of certain important options (see §3.2.2). A relative fraction of the flux at each line is assigned to each component, based on the derived fits, as discussed in §3.3. A flowchart of the POLYSTAR procedure appears as Fig. 2, in order to help clarify portions of the subsequent discussion.

3.1 Preliminary Considerations

As we can see from Fig. 2, there are two important decisions to be made before one applies the procedure to a given IUE image. First, the analyst must decide how many discrete components are present in the aperture and must provide an initial guess as to where their centers lie along the cross-dispersion axis. Secondly, he must also decide upon a particular wavelength bin configuration (the analysis is performed independently on each of several segments of the LBL file, which are recombined into a full spectrum as one of the last steps). In practice, both of these decisions are easier to make if one is able to see the entire LBL file in a single picture, such as a contour plot or a series of cross-cuts at specified wavelength intervals (see Fig. 3, for example). Such representations of the LBL data for each image help the user to make first guesses as to the number and location of the discrete components and to assess the overall signal-to-noise characteristics, a primary consideration in determining the proper bin sizes to use.

Several comments should be made here regarding one's choice of N, the number of components. First, one should try to use the *minimum* number of components for which "decent" fits are obtained in a majority of the wavelength bins. Clearly, one could fit just about any profile given enough degrees of freedom, *i.e.*, if $N = 4$ yields a credible fit then $N = 5$ will give you an even better one (see §4 for a detailed discussion of this issue). Secondly, there are a number of factors which can broaden the instrumental PSF, causing a single point source to appear as an unresolved blend of two or more stars (see §3.2.1). Finally, one should realize that unresolved clumps of stars may sometimes appear to be single point sources, as was found for several cases among the globular cluster images (Altner 1988a). Independent criteria are needed to interpret the data in these circumstances.

The "rule" we apply insofar as bin sizes is simple and obvious: for low signal-to-noise data one should use wide bins (50–100 Å) while for better quality data one should use narrower bins (25 Å). As we shall describe in §3.3, the weighting factors derived from the fits in a given bin are applied to all the samples in that bin, hence wide bins naturally translate into large uncertainties in the resulting spectra. POLYSTAR is set up to handle variable bin widths, should the signal-to-noise characteristics vary across the spectrum (see, for example, Altner and Heap 1988).

The spatial extent of sources in the large aperture varies from image to image, leading us to define an "effective aperture" along the LBL axis, which is always less than or equal to the size of the actual aperture. We determine the effective aperture for a given image by interactively measuring the line numbers of the left and right limits of the cross-dispersion profile, k_l and k_r, respectively.[4] Also, we would like to make a deliberate distinction between the terms "baseline" and "background". By "baseline" we mean a first or second degree polynomial fit to the data outside of the effective aperture in the *cross-dispersion direction*. The baseline determined in each bin is subtracted from the cross-dispersion profile *prior* to

[4] In principle, since the PSF in all cameras is wavelength dependent, one might want to specify different limits for each bin. POLYSTAR was written with this option in mind. In practice, we found it more convenient to measure these limits once only, at the widest point in the LBL spectrum.

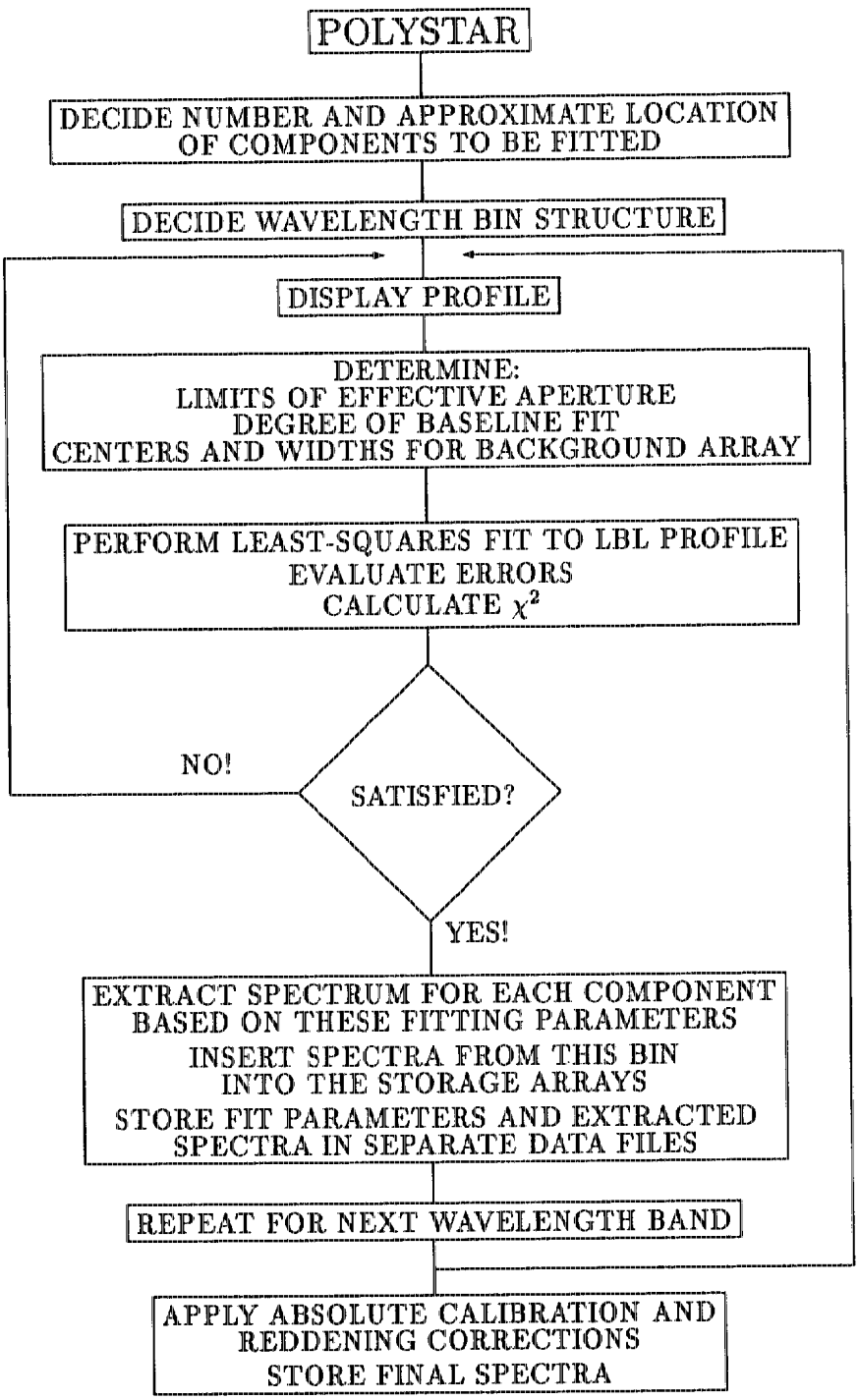

Figure 2: Flowchart of the POLYSTAR multi-component extraction procedure.

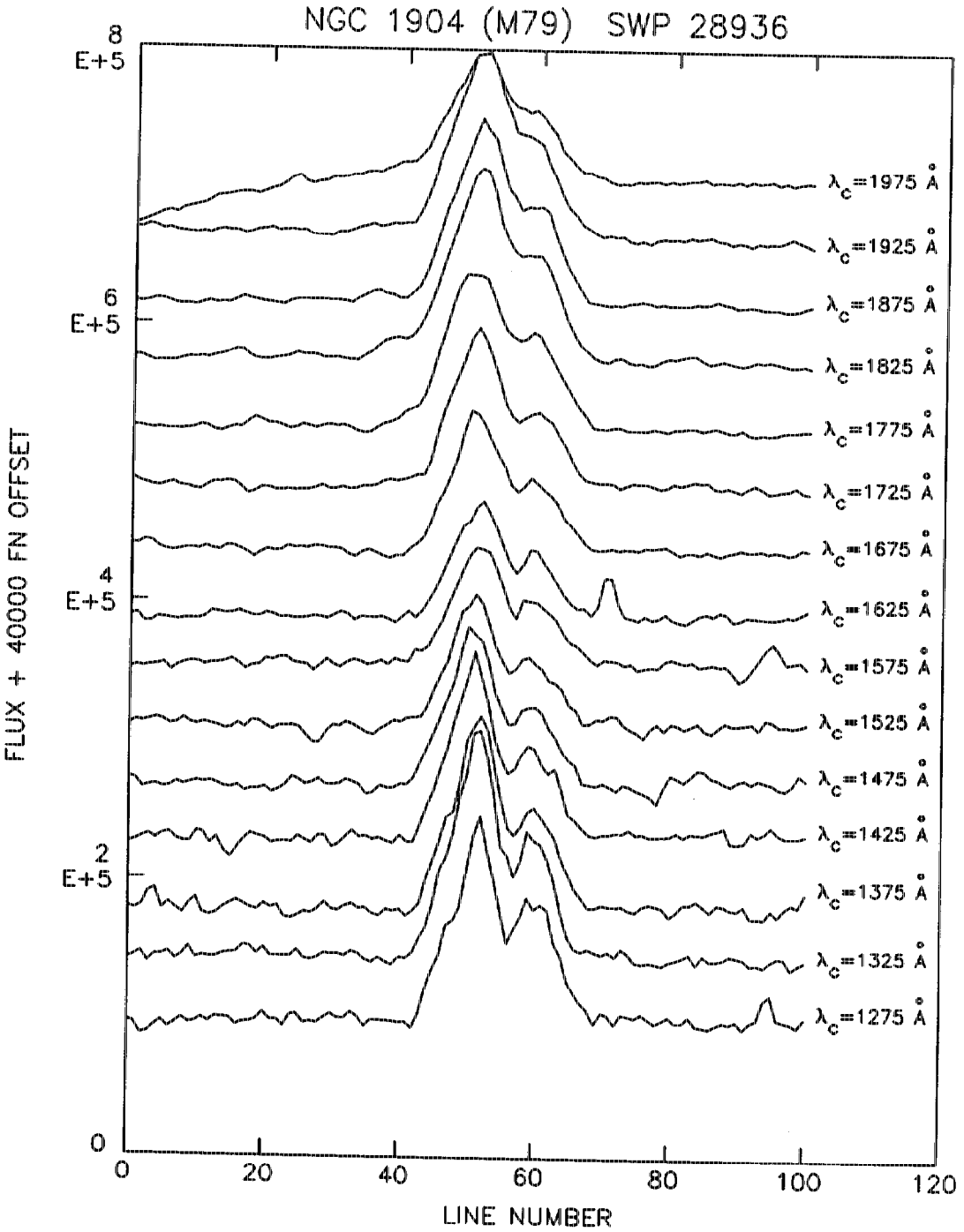

Figure 3: Cross-dispersion profiles from SWP 28936 (NGC 1904).

attempting the fit to N components (the χ^2 of the baseline fit is a useful number to consider in evaluating the χ^2 of the N component fit, since it is a good measure of the rms noise level of the data. The "background", in contrast, is measured along the *dispersion* direction. Data in a default set of lines outside the effective aperture are summed, smoothed using median and boxcar filters to remove spikes, and normalized to one line, then subtracted from the gross spectra to yield net spectra (see Eq. 12). This is the same prescription that is used in many of the RDAF routines.

3.2 Parameters of the Fit

In the original formulation of the POLYSTAR procedure we had assumed that the IUE cross-dispersion PSF is gaussian in shape, even though CBB had shown that better fits to the profiles of single point-sources could be obtained using a "skewed" gaussian function (for the SWP camera). Since the actual asymmetry is generally quite small (CBB estimate a difference of less than 2% in the integrated spectrum), our assumption appeared to be justified. Moreover, many other authors had likewise assumed a gaussian PSF for their extractions (deBoer and Code 1981; Caloi *et al.* 1984; Panek and Holm 1984) and we were thus further motivated to do the same in order to compare the POLYSTAR output to their results. However, in later self-calibration tests involving combinations of point-source spectra artificially shifted in line space to simulate complex cross-dispersion profiles, extractions using the gaussian form failed to adequately recover the *known* input spectra. Using the skewed gaussian PSF in these same tests resulted in substantial improvement in the accuracy of the separation procedure. We have therefore adopted the skewed gaussian as the preferred form of the SWP PSF.

Following CBB, we write the skewed gaussian function as

$$y(x) = \psi \exp\left\{-\ln 2\left[\frac{\ln[1+2\beta(x-\mu)/\gamma]}{\beta}\right]^2\right\} \quad \text{for } 2\beta(x-\mu)/\gamma > -1 \tag{2}$$

where

$$\gamma = \frac{\text{FWHM}\cdot\beta}{\sinh\beta} \tag{3}$$

and where

$$\text{FWHM} = 2\sqrt{2\ln 2}\,\sigma \tag{4}$$

as it does for the symmetrical gaussian. The function defined in Eq. 2 is zero outside the specified limits.[5] The parameter β measures the degree of asymmetry of the function, which takes the form of an extended wing, to the right for positive values of β and to the left for negative values. (The observed asymmetry in the SWP PSF is always positive.) As $\beta \to 0$ the function reduces to the symmetrical gaussian.

A skewed-gaussian representation of the cross-dispersion profile thus requires four parameters to be determined for each of the N components. We attempt to fit the data with the function

$$Y = \sum_{j=1}^{N} y_j = f(\mu_1,\sigma_1,\psi_1,\beta_1,\mu_2,\sigma_2,\psi_2,\beta_2,\ldots,\mu_N,\sigma_N,\psi_N,\beta_N) \tag{5}$$

[5]The independent variable x is treated as a continuous variable in Eq. 2 and in the POLYSTAR procedure. However, IUE LBL(ELBL) data actually consists of 55(110) points along the spatial axis. We use the discrete variable k to represent line numbers in those cases where it is important to make the distinction, such as the summation in Eq. 12.

where μ_j is the location of the peak of the jth component, *i.e.*, its "center",
σ_j is the width of the jth component,
ψ_j is the amplitude, or peak value of the jth component, and
β_j is the dimensionless skew parameter of the jth component.

Although the skewness was detected only in the SWP camera, use of the present form of the POLYSTAR procedure on long wavelength spectra is easily accomplished by setting $\beta_j = 0$ for each j (see §3.2.2).

3.2.1 Wavelength Dependence of the Parameters

Each one of the four parameters is wavelength dependent. This is not surprising in the case of the ψ parameter since it is a direct reflection of the actual spectrum. The wavelength dependence of the other three parameters is purely instrumental in origin, however, and each merits further discussion.

$\mu = \mu(\lambda)$ As the least-squares fitting portion of the POLYSTAR procedure evolved to its present form various options were added to allow control over each of the $4N$ parameters (see §3.2.2). The first option installed was a constraint on the locations of the peak centers. In the absence of information to the contrary, we made the reasonable assumption that once a good fit to the LBL profile in a particular bin was found, the fits in all the other bins should *require* the same set of component centers, $\mu = \{\mu_j\}$. Modifications were therefore made to the existing code, but the fits did not seem to improve much, if at all, and in many cases the derived stellar spectra exhibited gross discontinuities which we have since come to recognize as sure signs of errors in the assigned weight factors. Only later did we discover that there is, indeed, a residual wavelength dependence of the peak centers (*i.e.*, "curvature") in the low dispersion LBL images of all cameras. The severity of the curvature, as well as that of the related problem of spectral reseau motion, seems to depend on the spacecraft temperature and the camera exposure level (Thompson 1985).

The nature of the curvature problem is amply demonstrated in Fig. 4, which shows the variation with wavelength of the derived centers (in units of line number) for three components in SWP 9595 (NGC 5904). POLYSTAR fits were performed on each of the 25 Å wide bins, allowing the centers of all three components to be determined as free parameters. Note that the most significant deviations from the mean values (shown by the dotted lines) seem to occur at the same spectral locations for each component. This is quite typical behavior and is usually associated with either reseau or cosmic ray "hits" just outside the effective aperture, which apparently cause the readout beam to "bend" toward them. Notice that the separation *between* components, $\Delta\mu \equiv \mu_{j+1} - \mu_j$ $(j = 1, N-1)$, does not appear to be wavelength dependent.[6] The best cure for the curvature problem, as it applies to the POLYSTAR procedure, is to fix the relative offsets of up to $N-1$ components, but not to restrict the absolute location of the peak of the fiducial component in any way. The technique of using fixed offsets proved essential in the application of POLYSTAR to the images of SN 1987A (Sonneborn, Altner, and Kirshner 1987).

$\sigma = \sigma(\lambda)$ Convinced of the importance of telescope focus in spatial resolution studies of IUE low dispersion spectra, CBB were able to derive an improved description of the wavelength dependence of the PSF. Earlier studies, using spectra obtained with considerable variation in the focus STEP parameter, showed a large degree of scatter. Selecting only optimally focused spectra acquired though both large and small apertures, CBB were able to

[6] Our component numbering convention proceeds left to right across the cross-dispersion profile, such that $\mu_{j+1} - \mu_j$ is ways positive. The notation SWP 9595 C1 thus refers to the $j = 1$ component extracted from SWP 9595, *i.e.*, the star corresponding to the leftmost peak in the LBL file.

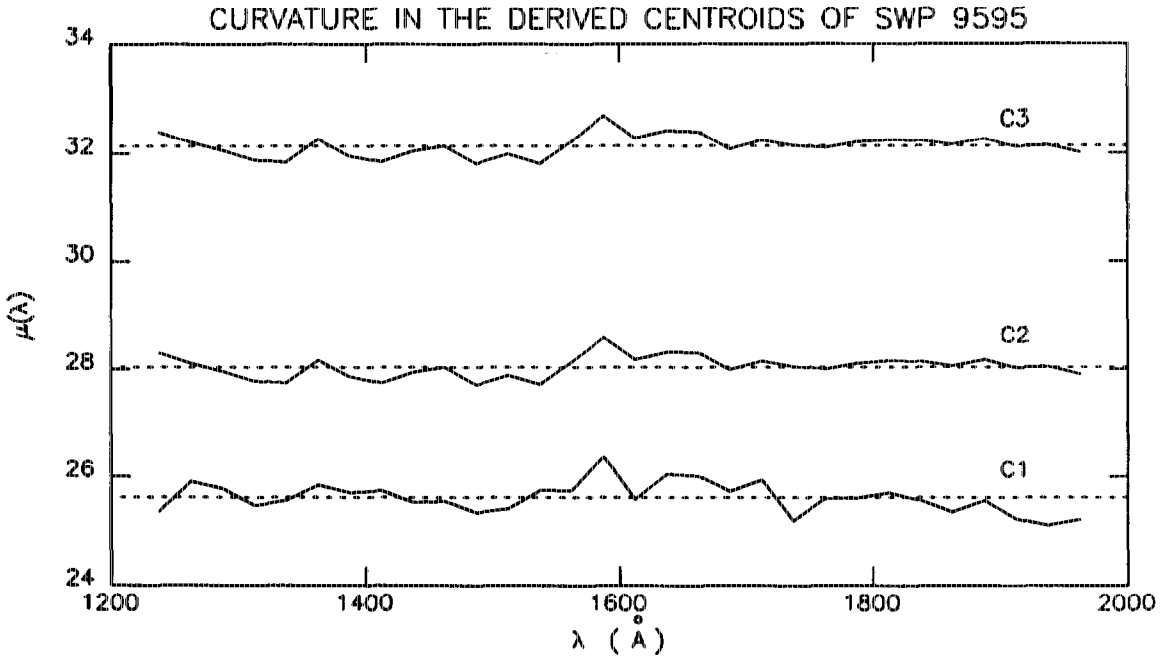

Figure 4: Wavelength dependence of the derived centers for each of the three components in SWP 9595, a typical example of "curvature" in the LBL data. The dotted lines show the mean position in each case. Significant errors in the final spectra result if a fixed position is used in all bins.

significantly reduce the scatter and define a reliable (±2%) mean function for each camera. We have adopted this mean curve as a "template" for use in the fitting procedure, after resampling to the appropriate bin spacing (CBB used 150 Å-wide bins).

Not all IUE images are obtained under conditions of perfect focus, however, and it is important to know how the PSF changes with changes in the STEP parameter. CBB studied this problem also and determined that the variation of the gaussian FWHM with focus is best described as a linear function for $3.5 > \mathrm{STEP} > 0$, and a flat "plateau" for $\mathrm{STEP} \leq 0$. But the slope of the linear portion of their curve, $\alpha = \Delta\mathrm{FWHM}/\Delta\mathrm{STEP}$, is itself wavelength dependent, having values of 0.33 and 0.23 at 1350 and 1850 Å, respectively.[7] From this information, and the arbitrary but reasonable assumption that a linear function describes the wavelength dependence of the slope, we have constructed a "correction algorithm" that allows us to obtain the FWHM at any STEP value, in any wavelength bin. In other words, we define a linear function such that

$$\alpha(\lambda) = \eta\,\Delta\lambda + \alpha_0 \tag{6}$$

where

$$\eta \equiv \frac{\alpha_2 - \alpha_1}{\lambda_2 - \lambda 1} = -2 \times 10^{-4} \tag{7}$$

[7]The quoted slopes are the reverse of those presented in Table 2b of CBB; however, from their Fig. 2a it is apparent that the slope of the 1350 Å function is steeper than that at 1850 Å. We have assumed that a typesetting error was made in the table.

and α_0 is the intercept at the beginning of the wavelength range ($\alpha_0 = 0.35$ at 1250 Å). From this one obtains

$$\mathrm{FWHM}(\lambda) = \alpha(\lambda) \cdot \mathrm{STEP} + \mathrm{FWHM}_0(\lambda) \tag{8}$$

where $\mathrm{FWHM}_0(\lambda)$ is the FWHM at optimum focus at wavelength λ.

In Fig. 5 we show the wavelength and focus dependence of the σ parameter for the SWP camera, obtained using Eq. 8 and the mean curve derived by CBB. We have converted from FWHM (in pixels) to σ (in LBL units) using the multiplicative factors listed in Table 1. The steady widening of the PSF for $\lambda > 1350$ Å for all values of the STEP parameter is ultimately attributable to the poorer focus of the camera readout beam, and is quite noticeable upon examination of the stacked cross-dispersion profiles in Fig. 3. CBB found the resolution of the SWP camera to be poorer than in either of the other two cameras at almost all wavelengths. They also found little difference based on which aperture was used.

As an example of the validity of Eq. 8 we cite the case of LWP 1565, one of the eighteen images of the double quasar 0957 +561 recently analyzed by Altner and Heap (1988). This image is listed in the VILSPA observing log as having a focus STEP value of +1.5. The mean projected separation between the A and B components was measured to be $5''.26 \pm 0.37$, using the unmodified CBB function. This value compared unfavorably with the predicted separation of $5''.87$, based on the positions of the two components given by Walsh, Carswell, and Weymann (1979), after accounting for the position angle of the large aperture. However, after applying Eq. 8 to the CBB function, a mean separation of $5''.76 \pm 0.36$ was measured from the POLYSTAR solution for this image. LWP 1565 was the only image of the eighteen for which the measured and the predicted separation did not agree (within the stated errors)

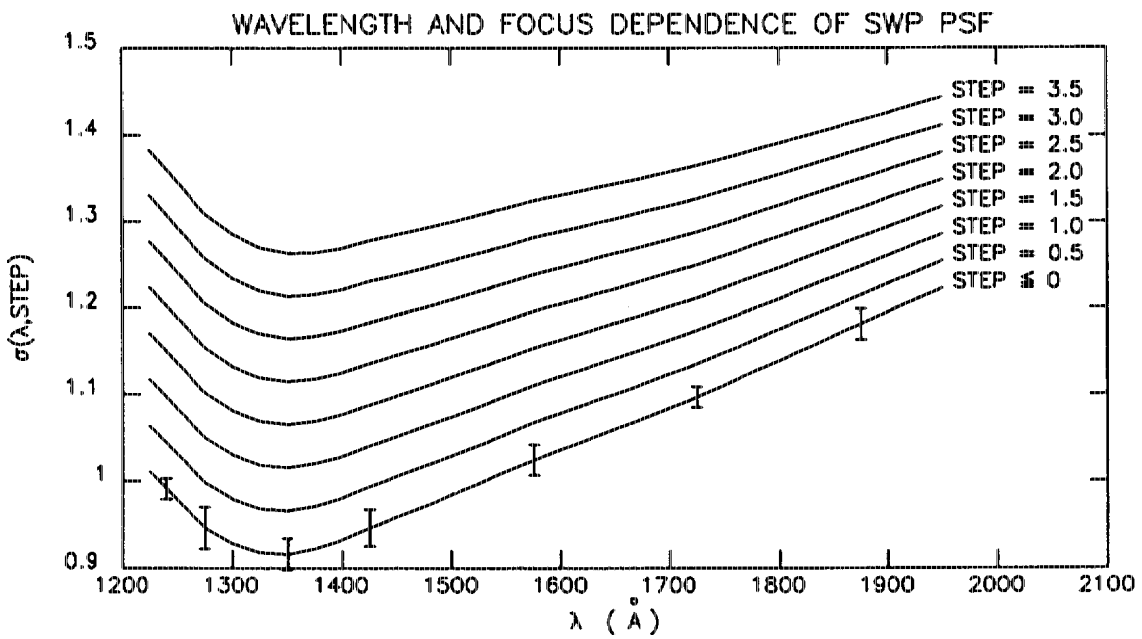

Figure 5: Wavelength and focus dependence of the PSF width parameter obtained using Eq. 8 for the SWP camera. LBL units are used for σ and the error bars are from CBB, for the case of optimum focus. Note the pronounced minimum near 1350 Å.

when the CBB function was used. Most significantly, it was also the only one to have been observed at less than optimum focus.

Poor camera focus is not the only mechanism by which the PSF of a source is broadened beyond that given by the CBB curve. Target drift in the aperture can occur during long exposures, especially if the ecliptic latitude of the source is large and no star brighter than 13th or 14th magnitude within 7′ of the target is available for the FES to guide on (Sonneborn *et al.* 1987). In such cases the observer needs to periodically interrupt the exposure and recenter the target in the aperture. We stress that long exposure times do not *necessarily* cause broadening. The IUE data archives contain many excellent examples of long-integration-time images of faint point sources for which the PSF is quite close to the unbroadened CBB curve. Ultimately, one must go back to the original observing script in order to determine whether or not target drift problems arose during any given exposure, and, if so, what steps were taken to minimize them. An additional option in POLYSTAR allows one to apply a multiplicative scale factor to the width parameter if this is deemed necessary. This "correction" increases the width of the PSF but does not change its wavelength dependence.

$\beta = \beta(\lambda)$ Asymmetry in the SWP cross-dispersion profiles was first pointed out by Snijders (1980). CBB compared the fits obtained with both the symmetric and the asymmetric gaussian function for a few selected IUE point-source spectra, in order to provide an accurate analytical representation of the PSF. For the SWP case they used two spectra of BD +28 4211 which were obtained at conditions of optimum focus, reprocessed to take advantage of the superior spatial resolution of the ELBL format, and averaged in 50 Å wide bins. In both cases the skewed gaussian fit was "decidedly a better representation for the SWP profiles" and showed very similar wavelength dependence of the skew parameter, confirming that β "actually describes an optical property of the spectrograph".

Several factors prompted us to attempt verification of the shape of the skewness function as it was presented in CBB. First, they did not present the data in a table as they had for the σ parameter, and we were therefore forced to estimate the values from a small figure (their Fig. 10). Moreover, having deduced this function from only two spectra, they were unable to quote reasonable uncertainties. Lastly, the POLYSTAR procedure is well suited to such an analysis, so no additional software development was necessary. We measured the skewness in fourteen images of bright IUE calibration stars, all obtained through the large aperture and all at optimum focus, using 25 Å-wide bins. The results of that study are shown in Fig. 6. The solid line in that figure is our adopted mean skewness function, and the error bars show the 1σ scatter about the mean. The dotted curve and the dashed curve show the (interpolated) CBB function for the large and small aperture, respectively. Although the scatter in our curve is larger than we would like, the three curves agree well enough to convince us that we have, indeed, measured a repeatable phenomenon. We have adopted our mean function as the best representation of the SWP skewness, to be used in situations where the complexity of the spatial profiles would prohibit its determination as a free parameter, as discussed in the next section.

3.2.2 Constraining the Parameters

The "best" fit in the sense of the formal least-squares method is that combination of parameters which yields the minimum χ^2. However, all of the parameters which describe the fitting function need not be *free* parameters. Given some *a priori* knowledge of possible limits to the value of a parameter, one would naturally want the solution to include that information, otherwise the fit would be meaningless, even though it might match the data exactly. Therefore, in order to take advantage of our knowledge of the instrumental properties which pertain to spatial resolution, or to incorporate spatial or spectral information we might have about the target itself, we installed additional options in the POLYSTAR

code which allow control over the values of any one or more of the $4N$ parameters. For example, we may wish to specify the value of a parameter in one or more bins explicitly, or we may find it useful to fix the value of a parameter for one component relative to the value for another component. We have discussed one example of the latter type in §3.2.1, in connection with the problem of curvature in the component centers. A similar approach was used to control the flux *ratio*, ψ_2/ψ_1, in a few of the SN 1987A spectra (Sonneborn, Altner, and Kirshner 1987).

A typical example of the need for *absolute* constraints is shown in Fig. 7, which illustrates several attempts to fit the profile of SWP 15892 (NGC 5904) in the wavelength region 1700–1750 Å. In all four figures the open circles represent the data (after baseline removal), while the solid curve represents the least-squares fit to that data. The dashed curves show the derived individual component profiles which, when added together, constitute the overall fit. The filled squares denote the residuals (data - fit), which are zero at the position of the horizontal line. Although the data is the same in all four cases, the conditions under which the fit was obtained are quite different in each. In the first panel, Case *a*, the fit was obtained with no constraints, *i.e.*, all twelve parameters were determined within the least-squares procedure. In Case *b* the skew parameter for each of the three components was fixed at 0.25, the appropriate value for this particular bin from our mean curve. In Case *c* we again let β be a free parameter but required that $\sigma = 1.10$ lines, the unbroadened value in this wavelength region from the interpolated CBB function discussed in §3.2.1. Lastly, for the fit in Case *d*, we applied the constraints to both β and σ simultaneously. Initial "guesses" for the μ and ψ parameters were based on interactive measurement of the profile

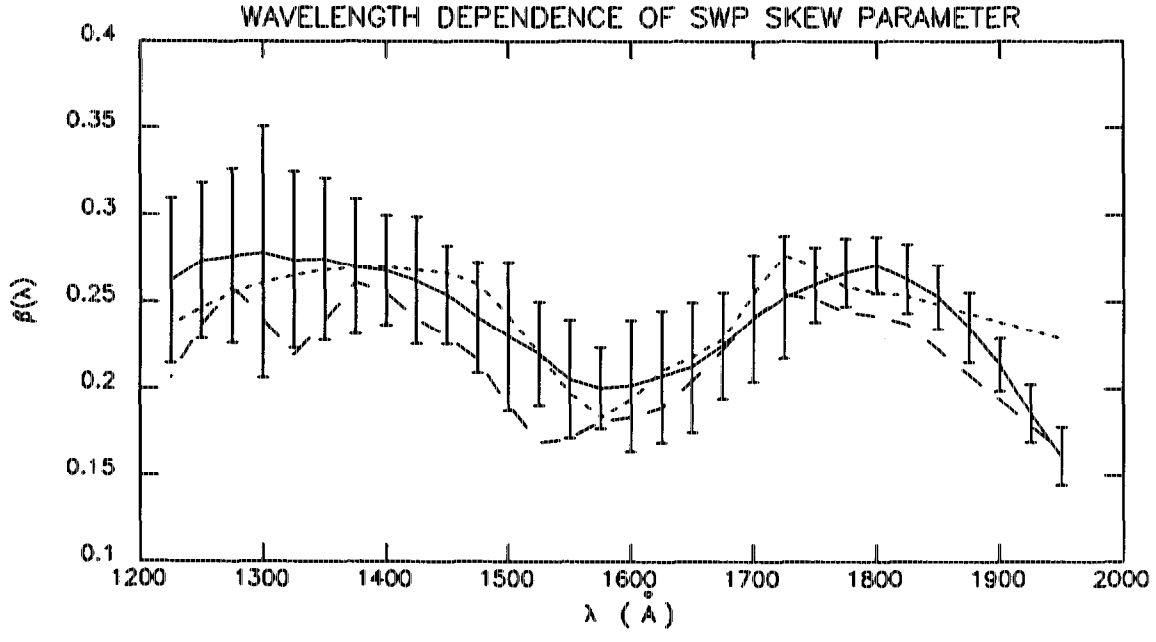

Figure 6: Wavelength dependence of the SWP skew parameter. The solid line is our determination of the mean skewness, based on fourteen images of IUE calibration stars. The error bars show the scatter about the mean for each of the 25 Å-wide bins. The dotted and dashed curves are based on the determination by CBB for large and small aperture images of BD +28 4211, respectively.

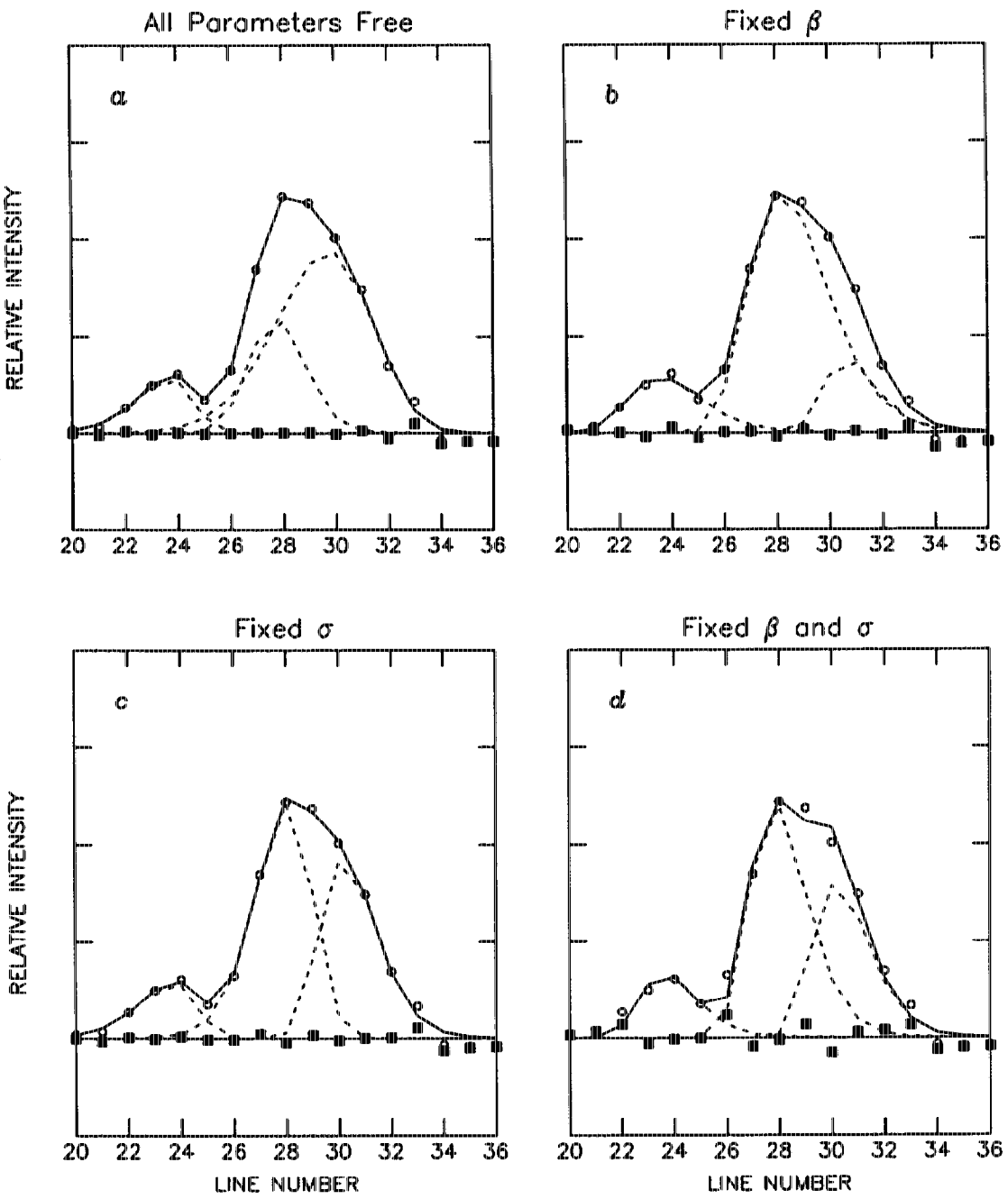

Figure 7: Least-squares fits to SWP 15892 (NGC 5904) in the 1700–1750 Å region. *a*) No constraints; *b*) β fixed for all three components; *c*) σ fixed for all three components; *d*) both β and σ fixed. Note that although the residuals (solid squares) are slightly larger in Case *d*, the solution is more realistic than the other three cases (see text and Table 2).

COMPONENT	μ	ERROR	σ	ERROR	ψ	ERROR	β	ERROR
Case *a*								
1	23.66	2.50	1.06	1.22	1.16E4	2.89E4	-0.32	1.43
2	27.72	1.44	1.07	3.01	2.39E4	1.95E5	0.08	3.12
3	29.71	6.35	1.84	6.39	3.77E4	5.76E4	-0.16	2.34
Case *b*								
1	23.53	0.92	1.40	1.06	1.16E4	5.00E3	0.25	-
2	28.26	0.78	1.51	0.75	4.97E4	7.66E3	0.25	-
3	30.65	0.78	1.02	0.96	1.51E4	2.62E4	0.25	-
Case *c*								
1	23.66	1.02	1.10	-	1.16E4	4.94E3	-0.35	1.15
2	28.03	0.29	1.10	-	4.85E4	6.92E3	-0.22	0.36
3	30.21	0.40	1.10	-	3.72E4	7.71E3	0.25	0.40
Case *d*								
1	23.61	0.51	1.10	-	1.33E4	4.42E3	0.25	-
2	27.81	0.19	1.10	-	4.86E4	5.86E3	0.25	-
3	30.18	0.29	1.10	-	3.18E4	5.90E3	0.25	-

Table 2: Three-component fits to SWP 15892 (NGC 5904): 1700–1750 Å. Fixed parameters are indicated by '–' in the error columns. As constraints are applied to one parameter, uncertainties in the other parameters are reduced.

and were the same in each case. In all four cases the fits are "good", in that the residuals are very close to zero, but the spectra one would derive from the individual component profiles would be significantly different (see §3.3). The actual values of the parameters determined for each component in each case, and the attendant uncertainties, are shown in Table 2.

We note in Case *a* and Case *c* that two of the components show *negative* skew values (*i.e.*, the extended wing of the asymmetric function is leftward of the peak center), whereas the asymmetry in the SWP profiles of single point-sources is always observed to be positive. Furthermore, the errors associated with these values are unacceptably large. We conclude that while skewness is definitely present in the SWP data and should not be ignored, it is a mistake to treat it as a free parameter under these circumstances. Instead, we henceforth assume that the mean curve shown in Fig. 6 is valid at all lines along the cross-dispersion axis, and we require that all component profiles in a given bin have the same skewness.

Similar misgivings obtain with regard to treating the profile widths as free parameters, even when the skewness is held fixed. In the absence of evidence that halation plays a role (*i.e.*, broader profiles with increasing flux level), one would expect the widths to be the same for all three components, if they are true point sources. This is not found in Case *b*, unless one allows for the rather large uncertainties associated with each measurement. Note that the derived values are almost 50% larger than those predicted by CBB for the first two profiles, which suggests that each of them might be further split into two components. However, by fixing σ, requiring it to be the same for each component, we obtain a perfectly acceptable three-component fit to the data in this bin (Case *d*). Note also that the uncertainties in the μ and ψ parameters are substantially smaller in Case *d* than they were in the first three fits.

We stress that the above example for SWP 15892 is typical in its general features. We always constrain the width and skewness to the appropriate values, taking advantage of the known properties of the instrument. Further controls are usually unnecessary, except in the noisiest data, whereupon we might specify relative offsets for the peak centers, determined from an earlier run. Naturally, it sometimes happens that, no matter how we force it, we cannot achieve acceptable fits in a majority of the bins. When this occurs we are forced to

consider fitting to $N' = N + 1$ components (however, see §4). One of the surest signs that we have underestimated the actual number of peaks is the occurrence of anomalously large residuals at the same spatial location in most of the bins, even after allowing for a slightly broader PSF than that described by CBB.

3.3 Assigning the Relative Weights

Once the skewed gaussian profiles for each component are determined in a particular wavelength bin they serve as "extraction slits" in the following sense. Each individual component profile is described by a set of array elements g_{jk} ($k = 1, 2, \ldots, 55$ for LBL files and $k = 1, 2, \ldots, 110$ for ELBL files) which are essentially zero outside the specified limits of the effective aperture and non-zero inside of these limits. We then define,

$$G_k \equiv \sum_{j=1}^{N} g_{jk} \tag{9}$$

such that,

$$f_{jk} = g_{jk}/G_k \tag{10}$$

is the relative weight of the jth component at line k. The above normalization condition implies that,

$$\sum_{j=1}^{N} f_{jk} = 1 \tag{11}$$

which is a statement of a kind of "conservation of flux" principle, in the sense of the phrase "robbing Peter to pay Paul". This is an important consideration in helping to evaluate the results of the component separation in particularly noisy bins or otherwise difficult cases, since assigning too large a weight to one component results in a correspondingly low weight for an adjacent component. In the final combined spectrum such pathologies are usually signaled by the occurrence of abrupt discontinuities at bin boundaries. We show examples of this "Peter-to-Paul" effect in §4.

We employ the weights defined in Eq. 10 as multiplicative constants in the summation step in order to derive the net extracted spectrum. In the *standard* IUESIPS extraction of a point-source from the LBL (ELBL) file the data arrays are simply summed over 9 (18) lines. From this "gross" spectrum an appropriate mean background array, scaled to the proper slit width, is subtracted to obtain the net spectrum. In the case of aperture-filling, multiple sources, however, we derive the spectrum for component j by summing over the limits of the effective aperture, after multiplying by the derived relative weight:

$$\vec{F}_j = \sum_{k=k_l}^{k_r} f_{jk}(\vec{d}_k - \vec{b}) \tag{12}$$

where k_l and k_r are the left and right limits of the effective aperture, respectively, determined prior to the fitting procedure, where $\vec{d}_k$ is the gross spectrum at line k, and where $\vec{b}$ is the mean smoothed background array, normalized to one line. For an unblended point source this reduces to the IUESIPS standard extraction (if k_l and k_r are properly chosen), since the weighting factor $f_{1k} = 1$ for all k. We use vector notation in the above to denote quantities which are arrays along the *dispersion* direction. As the data in each bin is analyzed, the net extracted spectrum for each component in that bin is inserted into a storage array which holds the results of extractions in previous bins. After data in the last bin has been processed and stored the complete spectrum can be retrieved for further analysis, along with the appropriate epsilon array. Data pertaining to the fits in each bin are stored in a separate file for later review, if necessary.

3.4 Errors and Uncertainties

Throughout the discussion of the POLYSTAR procedure in the preceding pages we have alluded to various assumptions which were made in order to be able to separate the overlapping profiles in the LBL data. Here we shall summarize what we believe are the major uncertainties of the procedure and how they ultimately affect the extracted spectra. Three broad categories of uncertainty delineate (with some overlap) the major concerns, namely *i*) the quality and reliability of the data, *ii*) the fitting procedure itself, and *iii*) the validity of assumptions incorporated into the procedure.

Factors affecting the reliability of the data, such as the effect of stray light from outside the aperture and light loss due to partial occultation by the aperture edges, are difficult to evaluate. Schiffer (1982) has estimated that a source contributes an amount proportional to $d^{-2.5}$, where d is the distance of the source from the center of the aperture ($40'' \geq d \geq 5''$). Carpenter *et al.* (1987) have studied the effects of diffraction spikes due to the mirror support structure. They concluded that significant extra flux is sometimes detected, depending upon the orientation of the large aperture with respect to the contaminating source. These effects are expected to be more important for extended sources than for point-like sources. The opposite problem of partial occultation can result in significant underestimates of the flux[8] (see Altner 1988b).

Particle hits both inside and outside the effective aperture region should be treated by pre-filtering the data in the dispersion direction. This helps to avoid incorrect estimates of the baseline level and component weight factors. The use of wide bins to compensate for low signal-to-noise is an unavoidable source of uncertainty, but is not a severe problem in the featureless continuum regions. Very broad bins inevitably result in some flux exchange (the Peter-to-Paul effect) due to the curvature problem, but the amount depends on the degree of separation between the components. Fortunately, this effect is easy to spot (if it is severe) and one or more of the constraints discussed in §3.2.2 can usually be applied to a troublesome bin to correct the problem.

The poorer spatial resolution of the LBL data, as compared to the ELBL data, is not as big a factor as one might imagine, given the use of mean width and skewness functions described earlier. ELBL profiles result in smaller errors in the derived spatial positions, of course, but we were able to obtain consistent results in a few cases where ELBL data became available after an LBL spectrum had been already been analyzed.

The second major source of uncertainty concerns the errors in the parameters reported by the POLYSTAR routine. These errors are a measure of the "curvature of the χ^2 hypersurface", in the words of Bevington (1969), being the diagonal elements of the error matrix. Bevington notes that the parabolic extrapolation used to approximate the curvature of the χ^2 hypersurface is somewhat sensitive to the starting points used in the search procedure. The approximation is valid only if the starting points are close enough to the local minima that higher order terms in the expansion become truly negligible. Our experience confirms this point; we have noted occasions where the procedure did not converge within the (self-imposed) limit of ten iterations, whereupon a change in the initial guesses resulted in convergence. In practice, we always estimate the peak centers as closely as possible, using a cursor on a graphics terminal. Also, as noted in the example of §3.2.2, constraining the values of certain parameters always reduced the errors of the remaining free parameters, and often solved the convergence problem as well. This amounts to a confinement of the

[8] Bruhweiler (private communication) estimates the fractional light loss to be

$$f_{out} \equiv \frac{I_{out}}{I_{tot}} = \frac{1}{2}\sum_{i=1}^{2}(1 - \mathrm{erf}(\frac{R_i}{\sqrt{2}\,\sigma(\lambda)}))$$

where R_i is the distance of the source from slit edge i and $\sigma(\lambda)$ is the gaussian width of the PSF, both measured in arcseconds.

search algorithm to a restricted portion of the χ^2 hypersurface.

Of course, the real issue of importance is how the quoted uncertainties affect the spectra. Not surprisingly, the weaker spectra are the most uncertain, especially if the degree of overlap with stronger sources is significant. Again the example in §3.2.2 can be considered typical; we see from Case *d* of Table 2 that the uncertainty in the peak height of the strongest component (C2) is only $\approx$ 12% while it is closer to 30% for the much weaker C1 component. Likewise, the ratio of the errors in the positions of the peak centers is roughly 3:1:2 for C1, C2, and C3, respectively, hence the positions of the weak components are also more uncertain than those of the brighter sources.

Lastly, let us consider several of the explicit assumptions in the procedure. For example, as we have shown above, the skewness parameter is an important element in the analytical description of the instrumental PSF, yet it cannot realistically be left as a free parameter in the case of severely blended multiple profiles profiles. Unfortunately, unlike the width parameter, the error bars for the mean β function are rather large. Uncertainties in the skewness have little effect for well separated peaks of equal amplitude, but as the degree of overlap increases so does the importance of having an accurate description of the shape of the PSF. Again, weak sources are most susceptible to large errors in the separated spectrum if the adopted mean skewness function is not truly representative, even more so if they happen to lie on the *right hand side* of a strong source in the SWP LBL image.

In §4 we discuss in some detail an approach to deciding the number of components to be fit in each image. The criteria there are both statistical and physical, but they are based on the belief that mechanisms which might broaden the profiles have been accounted for. In §3.2.1 we identified two such sources of broadening, telescope focus and target drift and we presented one example which suggests that the focus correction algorithm given there is probably valid. But we also note that during a long exposure the STEP parameter can change, so that the value obtained from the observing script (Goddard images) or observations log book (VILSPA images) may be somewhat uncertain. Scaling the CBB σ function as a "remedy" for target drift is, admittedly, quite arbitrary. Fortunately, the situations where these two mechanisms might cause confusion are relatively rare.

4 The Story of N

Let us now consider the problem of determining the "correct" number of components to use in a POLYSTAR fit to a given image. The simplest and most obvious approach is to use the *minimum* N that yields a "good" fit to the data, but since a better fit can always be obtained by including another component, at least in the sense that the residuals always become smaller, often the problem is one of knowing how good is good enough. Instrumental effects may complicate any attempts to separate closely spaced components, and might even mislead the analyst into believing that there are additional (weak) sources in the aperture. Even after adjusting the PSF for focus problems, there may be some residual ambiguity as to the best choice of N.

Because choosing a reasonable value of N is such a fundamental step in the POLYSTAR procedure, it is desirable to have at one's disposal certain criteria which might help in making the best choice. In this section we shall describe two "tests" of the hypothesis that N components is a better solution than the one which uses $N+1$ components. The first test is statistical in nature (the F test) which, when it works, allows one to accept or reject, at a certain confidence level, the reality of the additional component based on the relative improvement in the χ^2 of the fit. In the second test we attempt to determine whether the solutions with N and $N+1$ components give physically reasonable results, i.e., do the separated spectra resemble the spectra of real stars? This is the most important criterion, of course, and the answer we obtain in this way supercedes all other indicators.

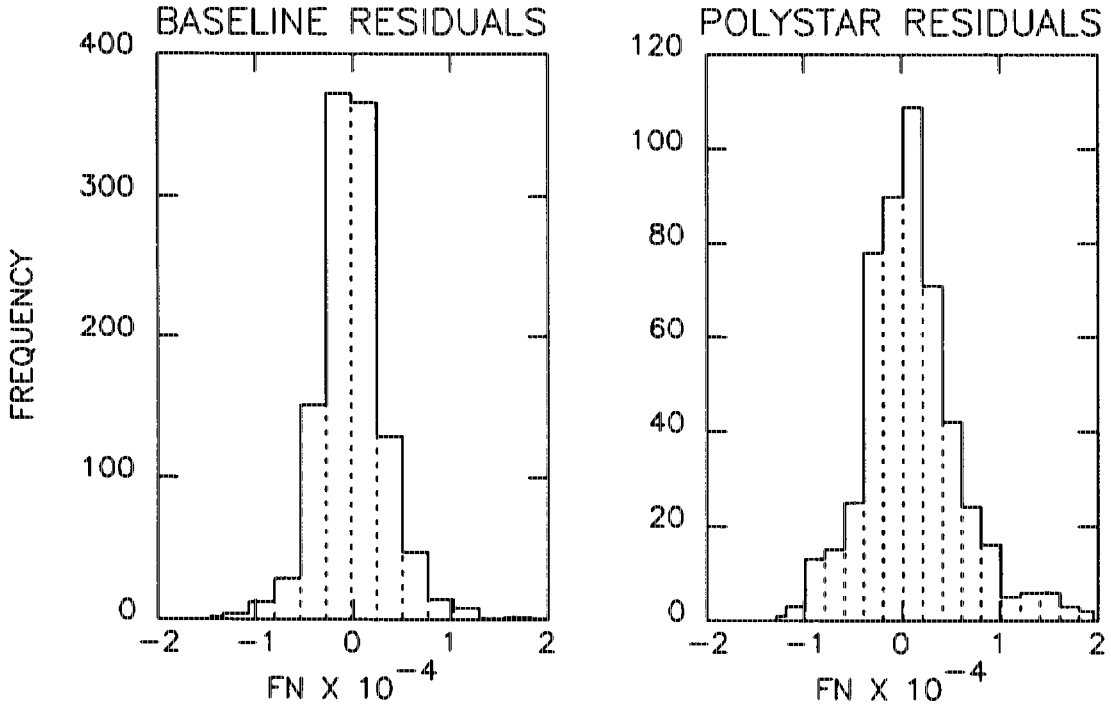

Figure 8: Normal distributions of the residuals from fits to both the baseline data (left panel) and data within the effective aperture (right panel). In both cases the residuals are from all thirty 25Å-wide bins in SWP 15313. The baseline data were fit to a quadratic, while the cross-dispersion profile data were fit using POLYSTAR, with $N = 4$. The normal distribution of the POLYSTAR residuals indicates that application of the F test may be appropriate in the present context.

4.1 The F Test

The residuals from fits to both the baseline data and the cross-dispersion profiles appear to be normally distributed (see Fig. 8), so the F test described by Bevington (1969) may be applicable to the problem mentioned above. The quantity F is usually defined as the ratio of two independent determinations of a *reduced* χ^2, i.e.,

$$f_{12} = \frac{\chi^2_{\nu 1}}{\chi^2_{\nu 2}} \tag{13}$$

where $\chi^2_{\nu 1} = \chi^2_1/\nu_1$ and $\chi^2_{\nu 2} = \chi^2_2/\nu_2$, with ν_1 and ν_2 being the number of degrees of freedom in the first and second cases, respectively. Here we are interested in the *difference* of two independently determined χ^2 statistics, which is also a χ^2 statistic:

$$F_{12} = \frac{\nu_2}{\nu_1 - \nu_2} \frac{\chi^2_{\nu 1} - \chi^2_{\nu 2}}{\chi^2_{\nu 2}} \tag{14}$$

If we let the POLYSTAR fit to N components be the first case and the fit to $N+1$ component be the second case, the ratio $F_{N,N+1}$ measures the relative improvement in the $N+1$ fit, and should be small if the improvement is not significant.[9]

[9]We adopt unit statistical weights in our calculation of χ^2, having no knowledge of what the true weights should be. Hence the "χ^2" that we determine is really the sum of the squares of the residuals. An alternate

ν_2	P=95%	P=99%	ν_2	P=95%	P=99%	ν_2	P=95%	P=99%	ν_2	P=95%	P=99%
2	19.00	99.00	8	4.46	8.65	14	3.74	6.51	20	3.49	5.85
3	9.55	30.80	9	4.26	8.02	15	3.68	6.36	21	3.47	5.78
4	6.94	18.00	10	4.10	7.56	16	3.63	6.23	22	3.44	5.72
5	5.79	13.30	11	3.98	7.21	17	3.59	6.11	23	3.42	5.66
6	5.14	10.90	12	3.89	6.93	18	3.55	6.01	24	3.40	5.61
7	4.74	9.55	13	3.80	6.70	19	3.52	5.93	25	3.39	5.57

Table 3: Critical F values for the case $\nu_1 - \nu_2 = 2$.

In applying Eq. 14 we must remember that although the fit to the spatially resolved data involves $4N$ terms, half of these are constrained, so that we really need to determine only two parameters for each component. In comparing the fits obtained using N and $N + 1$ components, we are therefore interested in the critical F values for the special case of $\nu_1 - \nu_2 = 2$, which we list in Table 3 for various values of ν_2 (for both 95% and 99% probability; data are from Lentner 1972). Derived F values greater than the tabulated values indicate that the additional component is statistically valid.

A representative example should clarify the issue. Consider the image SWP 26891, obtained at the center of light of NGC 6205. In Figs. 9*a–c* we display fits to the 1325–1350 Å bin of this image for the three cases of $N = 3$, 4, and 5, respectively. We see from the quality of the fits in these three cases that $N = 3$ is not a very good solution while $N = 4$ is better and $N = 5$ is (marginally) better yet. What does the F test tell us? With an effective aperture extending from lines 42–70, inclusive, we have $\nu_2 = 21$ and $\nu_2 = 19$ for the four and five component fits, respectively. Applying Eq. 14 to each bin of the fits for $N = 3$, 4, and 5 we display the distribution of F_{34} and F_{45} for SWP 26891 in Figs. 10 and 11. We see that the solution with $N = 3$ is rejected, with 29 of 30 F_{34} values exceeding the 99% critical value. But the solution with $N = 5$ is also rejected, as only 7 of 28 bins have F_{45} values above the 95% probability cutoff. The small negative values in a few bins actually tell us that the fits were *worse* with $N = 5$.

Thus, the F test is fairly reliable in rejecting those solutions which we knew to be wrong, or at least unlikely (i.e., the $N = 3$ solution for SWP 26891). Though not telling us anything new, at least it demonstrates how to interpret the run of F values. We also see that the F test can indeed help us to decide, with a fair degree of certainty, when to stop adding components.

4.2 Are the Separated Spectra Believable?

When applied to LBL data with 55 lines, instead of ELBL files with 110 lines, the results of the F test are not as clear-cut, due to undersampling (see Appendix D of Altner 1988a). In such circumstances it is unwise to put too much faith in statistical tests, and one must look for additional clues. One such clue is the appearance of the derived spectra, processed under the assumptions of $N = 5$ and $N = 4$, which we show in Figs. 12 and 13, respectively. Besides failing to converge within ten iterations in two bins, the 5-component solution yields spectra with obvious discontinuities (the Peter-to-Paul effect; see §3.3), an unambiguous indication of problems in the distribution of available flux. Combining the evidence from the statistical tests and from the spectra themselves, we are fairly certain that $N = 4$ is the best solution for the number of stars in the aperture of SWP 26891. The overall agreement

weighting scheme might be to use the variance in the baseline fit to normalize the χ^2 in each bin. In either case the F value calculated in Eq. 14 is not affected, since there we are interested in the *ratio* of two χ^2 distributions.

between the statistical and physical criteria allows some confidence that we have chosen the proper number of components in this image.

REFERENCES

Altner, B. 1988a, PhD. Thesis, Rutgers University.

Altner, B. 1988b, in *A Decade of UV Astronomy with the IUE Satellite,* Vol. 2, p. 189.

Altner, B. and Heap, S. R. 1988, in *A Decade of UV Astronomy with the IUE Satellite,* Vol. 2, p. 257.

Bevington, P. R. 1969, *Data Reduction and Error Analysis for the Physical Sciences,* McGraw-Hill, New York.

de Boer, K. S., and Code, A. D. 1981, *Ap. J. (Letters),* **243**, L33.

Bruhweiler, F. C., and Altner, B. 1988, in *A Decade of UV Astronomy with the IUE Satellite,* Vol. 2, p. 319.

Caloi, V., Castellani, V., Galluccio, D., and Wamsteker, W. 1984, *Astr. Ap.,* **138**, 485.

Carpenter, K., Stencel, R., Pesce, J., Brown, A., Judge, P., and Jordan, C. 1987, *NASA IUE Newsletter,* **33**, 20.

Cassatella, A., Barbero, J., and Benvenuti, P. 1985, *Astr. Ap.,* **144**, 335 (CBB).

Lentner, M. 1972, *Elementary Applied Statistics*, Bogden & Quigley, Inc., Tarrytown-on-Hudson, N.Y.

Muñoz Peiro, J. R. 1985, *NASA IUE Newsletter,* **27**, 27.

Panek, R. J. 1982, *NASA IUE Newsletter,* **18**, 68.

Panek, R. J. and Holm, A. V. 1984, *Ap. J.,* **277**, 700.

Reichert, G. A., Wu, C.-C., and Filippenko, A. 1988, in *A Decade of UV Astronomy with the IUE Satellite,* Vol 2., p. 307.

Schiffer, F. H. 1982, IUE internal memo.

Snijders, M. A. 1980, *SERC IUE Newsletter*, No. 5, p. 85.

Sonneborn, G., Oliverson, N. A., Imhoff, C. L., Pitts, R. E., and Holm, A. V. 1987, *NASA IUE Newsletter,* **32**.

Sonneborn, G., Altner, B., and Kirshner, R. P. 1987, *Ap. J. (Letters),* **323**, 35.

Thompson, R. W. 1985, in *Record of IUE Three-Agency Coordination Meeting*, Computer Sciences Corporation, CSC/TM-84/6173, pp. A-229.

Turnrose, B. E., and Harvel, C. A. 1980, *IUE Image Processing Information Manual*, NASA TM-79/6301.

Turnrose, B. E. and Thompson, R. W. 1984, *International Ultraviolet Explorer Image Processing Information Manual, Version 2.0*, Computer Sciences Corporation, CSC/TM-84/6058.

Walsh, D., Carswell, R. F., and Weymann, R. J. 1979, *Nature*, **279**, 381.

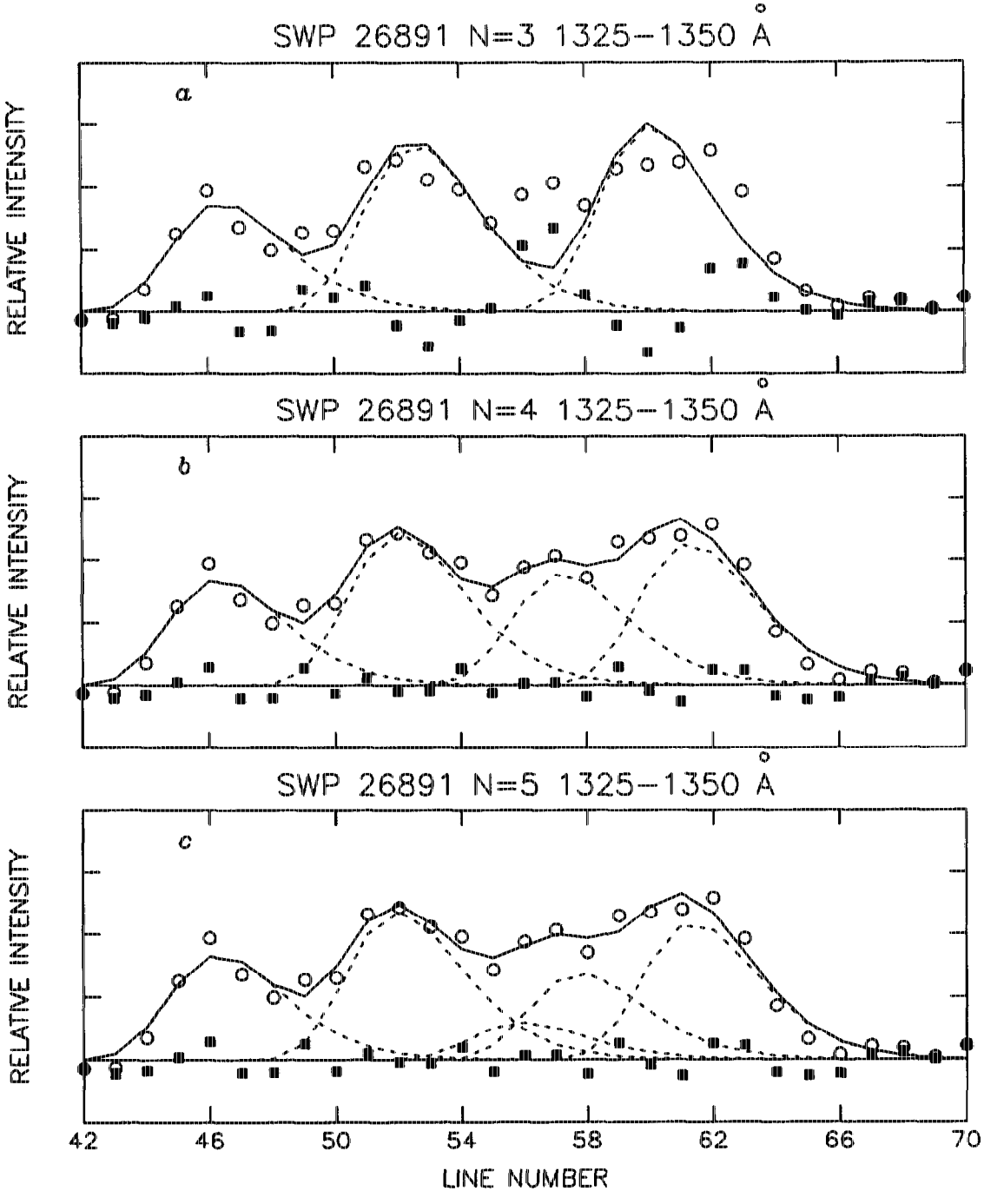

Figure 9: Fits to SWP 26891 (NGC 6205) in the range 1325–1350 Å for *a*) $N = 3$, *b*) $N = 4$, and *c*) $N = 5$. The improvement in using $N = 4$ relative to $N = 3$ is quite dramatic but similar improvement in using $N = 5$ over $N = 4$ is not seen. This conclusion is amply supported by the results of the F test (see text).

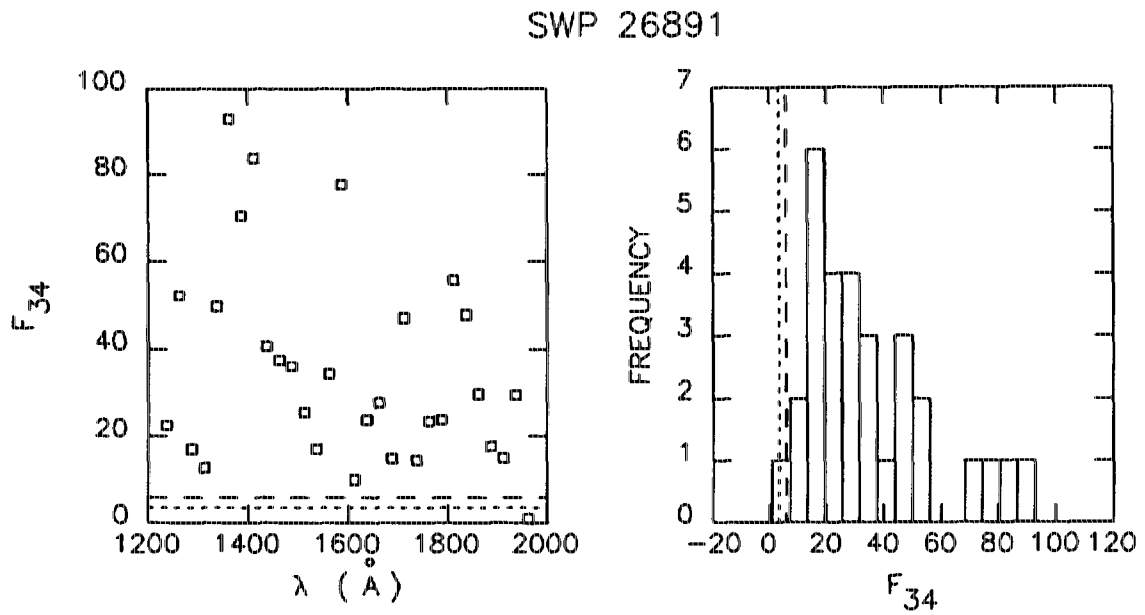

Figure 10: Results of the F test for $N = 3$ versus $N = 4$ in all thirty 25Å-wide bins in SWP 26891. The dotted lines at $F = 3.47$ and the dashed lines at $F = 5.78$ represent the critical values for 95% and 99%, respectively.

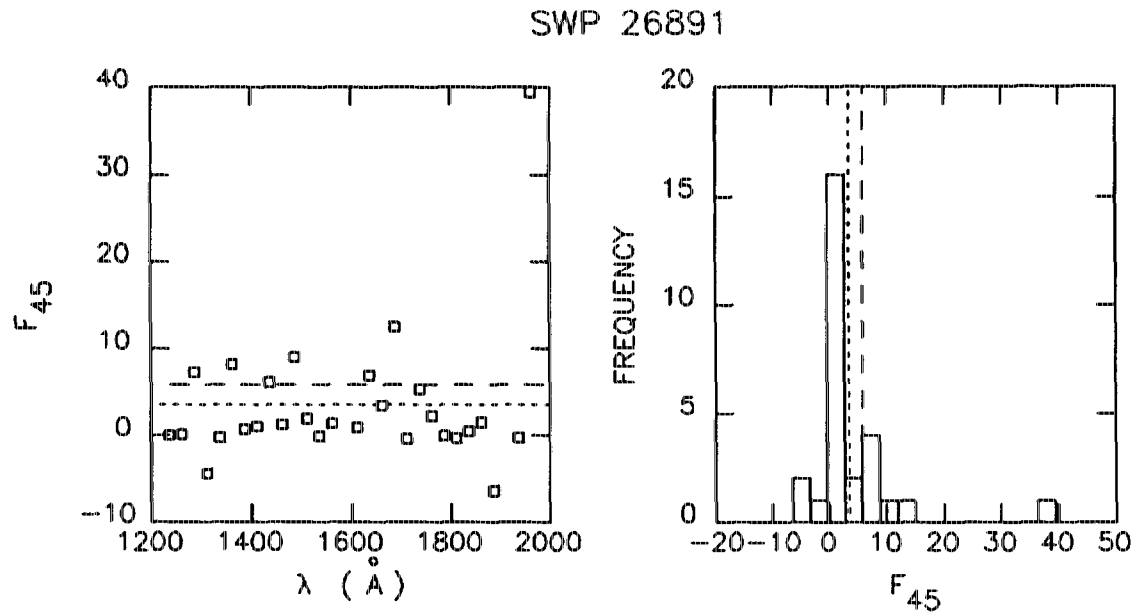

Figure 11: Results of the F test for $N = 4$ versus $N = 5$ in 28 of the 30 bins in SWP 26891 (POLYSTAR did not converge in two bins for $N = 5$). The dotted lines at $F = 3.52$ and the dashed lines at $F = 5.93$ represent the critical values for 95% and 99%, respectively.

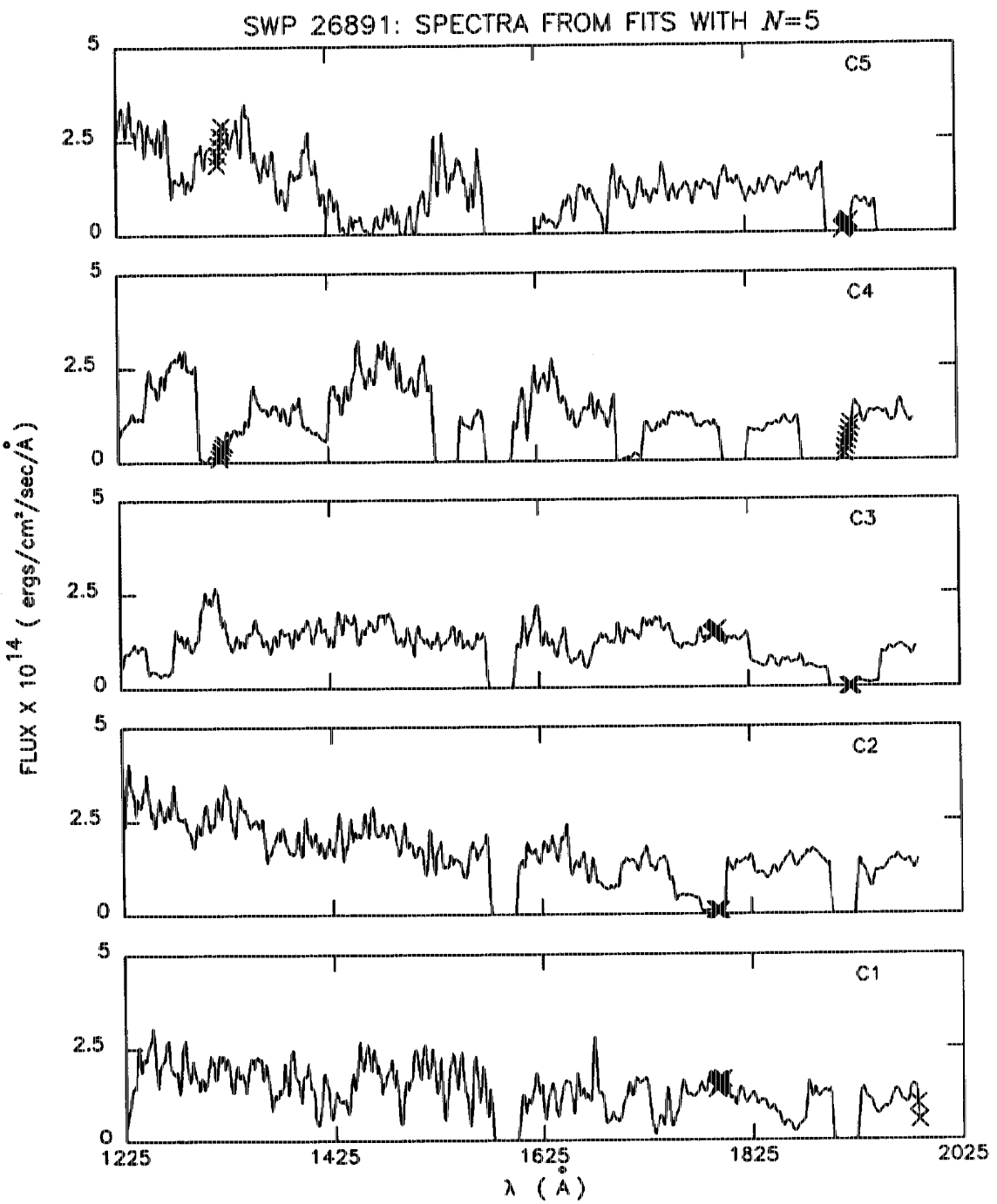

Figure 12: Spectra derived from POLYSTAR fits to SWP 26891 for 5 components. Note the sharp discontinuities and overall non-stellar appearance of the spectra. Such anomalies are a sure sign that we have tried to fit too many components to the cross-dispersion profile.

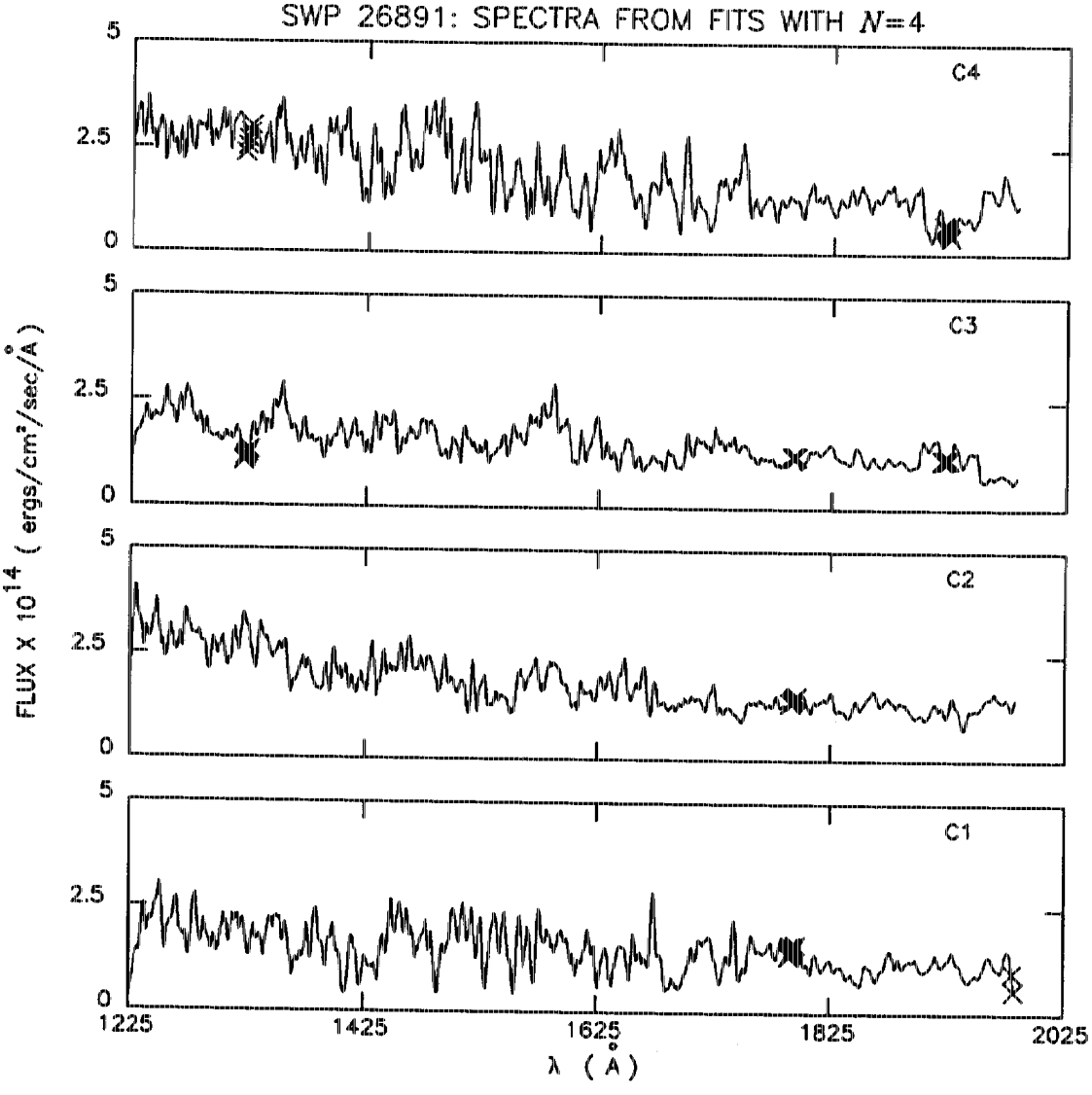

Figure 13: Spectra derived from POLYSTAR fits to SWP 26891 for 4 components. Though still somewhat noisy, the spectra displayed here are much more likely to represent those of real stars than those in Fig. 12.